OXFORD

Human Molecular Genetics 2018, Vol. 27, No. 16 2830–2839

doi: 10.1093/hmg/ddy191
Advance Access Publication Date: 16 May 2018
Original Article

ORIGINAL ARTICLE

Regulation of the neuropathy-associated *Pmp22* gene by a distal super-enhancer

Harrison Pantera[1,2], John J. Moran[1], Holly A. Hung[1], Evgenia Pak[3], Amalia Dutra[3] and John Svaren[1,4,*]

[1]Waisman Center, [2]Molecular and Cellular Pharmacology Graduate Program, University of Wisconsin-Madison, Madison, WI 53705, USA, [3]Cytogenetics and Microscopy Core, National Human Genome Research Institute, National Institutes of Health, Bethesda, MD, USA and [4]Department of Comparative Biosciences, University of Wisconsin-Madison, Madison, WI 53705, USA

*To whom correspondence should be addressed at: Waisman Center, University of Wisconsin-Madison, 1500 Highland Ave., Madison, WI 53705, USA. Tel: +1 6082634246; Email: john.svaren@wisc.edu

Abstract

Peripheral nerve myelination is adversely affected in the most common form of the hereditary peripheral neuropathy called Charcot-Marie-Tooth Disease. This form, classified as CMT1A, is caused by a 1.4 Mb duplication on chromosome 17, which includes the abundantly expressed Schwann cell myelin gene, Peripheral Myelin Protein 22 (*PMP22*). This is one of the most common copy number variants causing neurological disease. Overexpression of *Pmp22* in rodent models recapitulates several aspects of neuropathy, and reduction of *Pmp22* in such models results in amelioration of the neuropathy phenotype. Recently we identified a potential super-enhancer approximately 90–130 kb upstream of the *Pmp22* transcription start sites. This super-enhancer encompasses a cluster of individual enhancers that have the acetylated histone H3K27 active enhancer mark, and coincides with smaller duplications identified in patients with milder CMT1A-like symptoms, where the *PMP22* coding region itself was not part of the duplication. In this study, we have utilized genome editing to create a deletion of this super-enhancer to determine its role in *Pmp22* regulation. Our data show a significant decrease in *Pmp22* transcript expression using allele-specific internal controls. Moreover, the P2 promoter of the *Pmp22* gene, which is used in other cell types, is affected, but we find that the Schwann cell-specific P1 promoter is disproportionately more sensitive to loss of the super-enhancer. These data show for the first time the requirement of these upstream enhancers for full *Pmp22* expression.

Introduction

The integrity of the peripheral nervous system (PNS) depends on the coordination of peripheral nerve axons and the resident myelin-producing glia called Schwann cells. Axonal signaling to Schwann cells promotes myelination (1,2), and Schwann cells in return provide trophic support to axons (3) and enable the rapid saltatory conduction on which PNS function relies. This coordination is compromised in hereditary motor and sensory neuropathies of the peripheral nervous system, which comprise the family of disorders broadly called Charcot-Marie-Tooth disease (CMT) (4). CMT affects up to 1 in 2500 people (5) and is characterized by progressive distal limb muscle atrophy and weakness.

The most common subtype of CMT, called CMT Type 1A (CMT1A), accounting for 40–50% of CMT cases, results from a 1.4 Mb duplication on chromosome 17 which includes the myelin gene Peripheral Myelin Protein 22 (*PMP22*) (6–9). The reciprocal 1.4 Mb deletion is also linked to a second distinct disease, hereditary neuropathy with liability to pressure palsies (HNPP) (10).

Received: March 12, 2018. **Revised:** May 7, 2018. **Accepted:** May 9, 2018

Later transgenic studies linked aberrant *Pmp22* expression to peripheral neuropathy in rodent models of CMT1A (11), and studies of knockout alleles revealed symptoms in the *Pmp22* heterozygotes that resemble aspects of HNPP (12–14). Furthermore, in rodent models of *Pmp22* overexpression, reduction of the *Pmp22* transcript has been shown to ameliorate the symptoms of neuropathy (15–18), indicating that transcriptional regulation is a valid target of therapies for CMT1A, and drug screening assays have been set up to identify transcriptional modulators of *Pmp22* (19,20). Together, these studies highlight the importance of proper *Pmp22* gene dosage and a need to understand the endogenous regulatory mechanisms that establish and maintain this proper dosage.

The existence of distal regulatory elements for *Pmp22* was first suggested by transgenic studies of *Pmp22* promoter regions, which are able to drive low levels of Schwann cell expression of a reporter but are not greatly increased as the native gene is during the course of myelination (8,21,22). Subsequently, patients presenting with mild CMT-like symptoms were found to possess duplications of either 186 or 194 kb upstream of *Pmp22* but not including the gene itself (23,24). Within the 168 kb overlapping sequence shared by these duplications were a number of conserved noncoding sequences that could be potential regulatory elements (24). Accordingly, chromatin immunoprecipitation (ChIP) analysis identified high levels of H3K27 acetylation (H3K27ac) (25,26), a histone mark associated with active enhancers (27), and binding sites for transcription factors that regulate *Pmp22* and other genes in the myelination program (25,28,29), such as SOX10 (30,31), EGR2/KROX20 (32–35) and the Hippo pathway factor TEAD1 (29), within this distal region. Moreover, formaldehyde assisted isolation of regulatory elements (FAIRE) showed that the sites are found within open chromatin, which is another hallmark of enhancer regions. Finally, evidence from nerve injury models established a correlation between the status of these elements and *Pmp22* expression; following peripheral nerve injury, many of the H3K27ac marks within this region disappear (26), and there is a concurrent down-regulation of *Pmp22* transcription (36).

The most prominent SOX10/EGR2 binding sites within this region could drive expression in reporter assays (37). However, this work did not directly test if these putative enhancers, which are spread across approximately 30 kb and located around 100 kb away from the gene itself, contribute to *Pmp22* expression in their native genomic context. Therefore, we sought to test the contribution of this enhancer cluster by evaluating the consequences of inducing a deletion that would include these enhancers.

Results

Analysis of distal *Pmp22* enhancer region as super-enhancer

Genome-wide analysis of enhancers has identified large regions of noncoding DNA with the hallmarks of regulatory elements, called super-enhancers (38). Super-enhancers are defined as extended genomic regions that contain multiple constituent enhancers separated by <12.5 kb. A super-enhancer's constituent enhancers display enrichment of measures of enhancer status and function such as DNase I hypersensitivity, the enhancer-associated histone mark H3K27ac, and the binding of transcription factors at a higher degree than those found in typical enhancers. In general, super-enhancers are primarily involved in the regulation of genes essential for cell identity.

The enhancer-rich region upstream of the *Pmp22* gene was identified as a super-enhancer by assessing ChIP-seq occupancy of H3K27 acetylation. In the resulting distribution, 1694 super-enhancer domains were delineated from peaks corresponding to typical enhancers by establishing a threshold where the slope of the plot of super-enhancer score by ranked peaks exceeds 1 (Fig. 1A), and we selected a high confidence list of 1170 super-enhancers that have >1000 normalized reads (Supplementary Material, Table S1). Mapping of these peaks revealed an approximately 37 kb super-enhancer domain upstream of the *Pmp22* gene (hereafter referred to as Pmp22-SE) containing as many as six constituent enhancers, including previously described EGR2

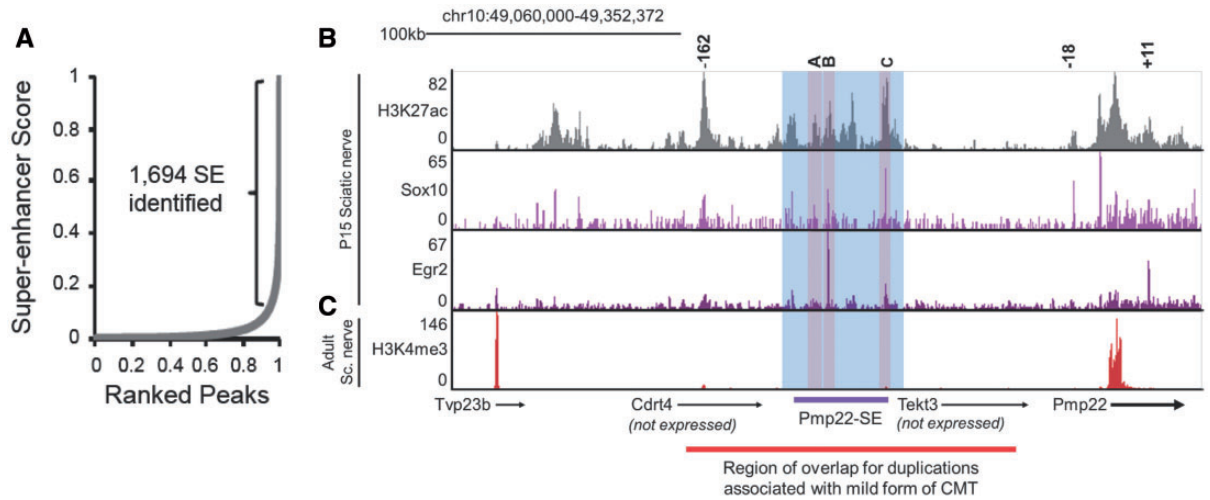

Figure 1. H3K27-marked super-enhancer Pmp22-SE coincides with a neuropathy-associated duplication. (**A**) Ranked occupancy of the enhancer-associated histone mark H3K27ac in P15 rat sciatic nerve identifies 1694 clusters of acetylation classified as super-enhancers. (**B**) ChIP-Seq analysis demonstrates that one super-enhancer, hereafter termed Pmp22-SE (purple bar), includes previously characterized enhancers A, B and C, located 120, 115 and 91 kb upstream of the *Pmp22* translation start site, respectively. Pmp22-SE coincides with a large region shared in overlapping duplications not including the *Pmp22* gene associated with CMT1A-like symptoms (red bar, rn5 chr10: 49, 146, 632–49, 288, 636, corresponding to hg36 chr17: 15, 143, 663–15, 311, 619). (**C**) ChIP-Seq analysis of H3K4me3, a histone mark associated with active promoters, in adult rat sciatic nerve indicates that Pmp22-SE-proximal genes Cdrt4 and Tekt3 are not expressed in peripheral nerve. The blue shaded region indicates the area targeted for deletion using CRISPR-Cas9.

and SOX10 binding sites labeled A, B and C (Fig. 1B). This domain falls within the smallest region of overlap for the previously-described intergenic duplications associated with mild forms of CMT (24). Analysis of an existing adult sciatic nerve ChIP-seq data set (39) for H3K4 trimethylation (H3K4me3), a histone mark associated with active promoters (40), was used to evaluate activity of nearby genes (Fig. 1C); these data demonstrate that the two genes nearest Pmp22-SE, CMT1A duplicated region transcript 4 (*Cdrt4*) and Tektin 3 (*Tekt3*), are transcriptionally silent in peripheral nerve, and that the closest expressed genes are *Pmp22* and trans-golgi network vesicle protein 23 homolog B (*Tvp23b*), a gene of unknown function.

Deletion of Pmp22-SE by CRISPR-Cas9

To evaluate the *in situ* function of Pmp22-SE, we employed the CRISPR-Cas9 system to induce a large deletion that would remove the major enhancers within Pmp22-SE. As has been demonstrated previously (41), the simultaneous induction of double-stranded breaks at two points on the same chromosome by CRISPR-Cas9 complexes can be used to trigger a large deletion of the intervening sequence. We used the same approach to delete Pmp22-SE in a modified clone of the S16 rat Schwann cell line. The rat S16 Schwann cell line is a useful experimental model for studying myelin gene expression because it expresses several myelin genes, including *Pmp22*, at levels near those found in myelinating Schwann cells *in vivo* (42). Moreover, studies of regulation in the S16 cell line have shown many similarities in transcription factor binding in the S16 cell line compared to *in vivo* ChIP analysis of rat peripheral nerve (29,34,37,43,44).

Since deletion may not occur readily on all copies, we chose to use a variant clone of the immortalized S16 rat Schwann cell line (45) in which one of the *Pmp22* alleles contains two reporters inserted by genome editing (Fig. 2A). Similar clones were prepared for reporter-based drug screens (19), and the firefly luciferase and secreted nanoluciferase reporter open reading frames are separated from the Pmp22 open reading frame and from each other by intervening 2a ribosome stuttering sequences (46). Sequencing of PCR products spanning the insert junctions showed that reporters had been incorporated just downstream of the *Pmp22* open reading frame in the last exon (Supplementary Material, Fig. S1A). However, the 3′ UTR of the *Pmp22* gene is retained in order to minimize any changes to transcript stability and processing. As *Pmp22* is transcribed along with the reporters in a single mRNA on this copy, we can use quantitative RT-PCR to distinguish between the two resulting species of *Pmp22* allele, (henceforth referred to as either the wild-type or reporter alleles).

Using this S16 clone with a reporter-tagged allele, the deletion of the super-enhancer was created by transfecting with plasmids that express both the Cas9 protein and the sgRNA targeting sequences approximately 38 kb apart. Included within this region are the previously-analyzed elements A, B and C at −120 kb, −115 kb and −91 kb, respectively, as well as a potential elements marked by H3K27ac at −128 kb, −108 kb, and −104 kb. Using primer combinations that flank the anticipated repair

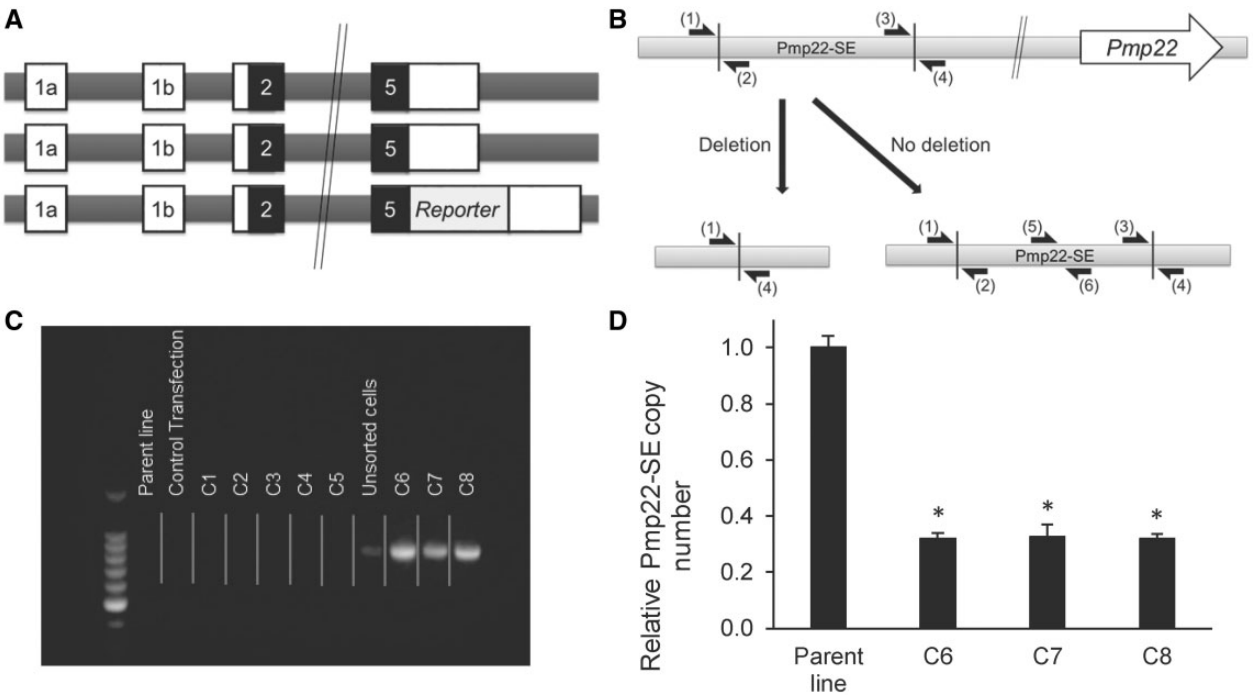

Figure 2. Simultaneous CRISPR-Cas9 application induces multi-copy deletion of Pmp22-SE. (**A**) Schematic of the *Pmp22* locus in the cell line used for this approach. *Pmp22* constitutes six exons, including non-coding alternative first exons 1A and 1B. White regions indicate non-translated portions of exons; black regions indicate translated portions of exons. A modified derivative of the S16 rat Schwann cell line was developed in which one allele of Pmp22 includes a reporter cassette inserted at the end of the last exon of *Pmp22* on one of the three copies of the Pmp22 gene. (**B**) Cells transfected with the CRISPR-Cas9 expression constructs are tested for successful deletion by pairing primers that flank each individual target site (indicated by arrows at positions 1 and 4). The number of copies of chromosome 10 possessing the deletion is evaluated by quantitative PCR of genomic DNA using primers within the deletion (e.g. those at positions 5 and 6) as well as a region outside of the deletion, found 74 kb upstream of the *Pmp22* translation start site. (**C**) PCR amplification of the repair junction was used to detect the deletion in CRISPR-Cas9-transfected unsorted cells and in clones C6, C7 and C8. (**D**) Evaluation of copy number of the deleted region relative to a nearby segment outside of the deleted region using the Comparative Ct method. Error bars represent the standard deviation of four technical replicates (*$P < 0.05$).

junction resulting from deletion of Pmp22-SE (Fig. 2B), we successfully amplified a unique PCR product resulting from this deletion in the pool of transfected cells as well as in a subset of clonal lines isolated from this pool by single-cell sorting (Fig. 2C). The anticipated repair junction was confirmed using Sanger sequencing (Supplementary Material, Fig. S1B). Screening of 72 clonal lines yielded eight clones in which the deletion could be detected. However, we could also amplify a PCR product with primers flanking each individual sgRNA targeting site in these clones (data not shown), indicating that we did not achieve homozygous deletion of Pmp22-SE on all copies of chromosome 10.

Karyotyping of the S16 cell line revealed that the line is polyploid, with an average of three copies of each chromosome, including chromosome 10 where the *Pmp22* gene is located (Supplementary Material, Fig. S2). To determine the number of copies possessing the deletion in each clone, quantitative PCR was performed using two primer sets targeting separate regions both inside and outside of the target region (Fig. 2D). Representative results from the parent reporter line were compared to results from three clones C6–C8 in which the deletion could be detected. Clones C6–C8 displayed normalized copy number reduction of approximately 70% compared to the average value of clones C1–C5, suggesting that these clones possess deletions of Pmp22-SE on two of the three copies of chromosome 10.

Pmp22-SE is required for full *Pmp22* expression

Since the overall level of Pmp22 expression was reduced in these clones (not shown), we aimed to determine if this effect was allele-specific, since that would provide a useful internal control for the potential obfuscating effects of clone-to-clone variation in *Pmp22* expression. Levels of *Pmp22* mRNA were determined via quantitative real-time reverse transcription PCR (qRT-PCR) using primers that differentiate the wild-type and reporter alleles (Fig. 3A). Using this method, we found that the three clones C6–C8 presented here displayed an approximate two-fold reduction in *Pmp22* transcription exclusively on the wild-type alleles relative to the five 'deletion-negative' clones C1–C5 when normalizing the results to the housekeeping gene *Actb* (Fig. 3B), indicating that this super-enhancer is required for full activation of *Pmp22* transcription. In contrast, the expression of the reporter allele was not affected, indicating that the deletions on 2 of the 3 copies occurred on the wild-type alleles of *Pmp22*.

As the negative clones C1–C5 show some evidence of variation in myelin gene regulation such that *Pmp22* expression

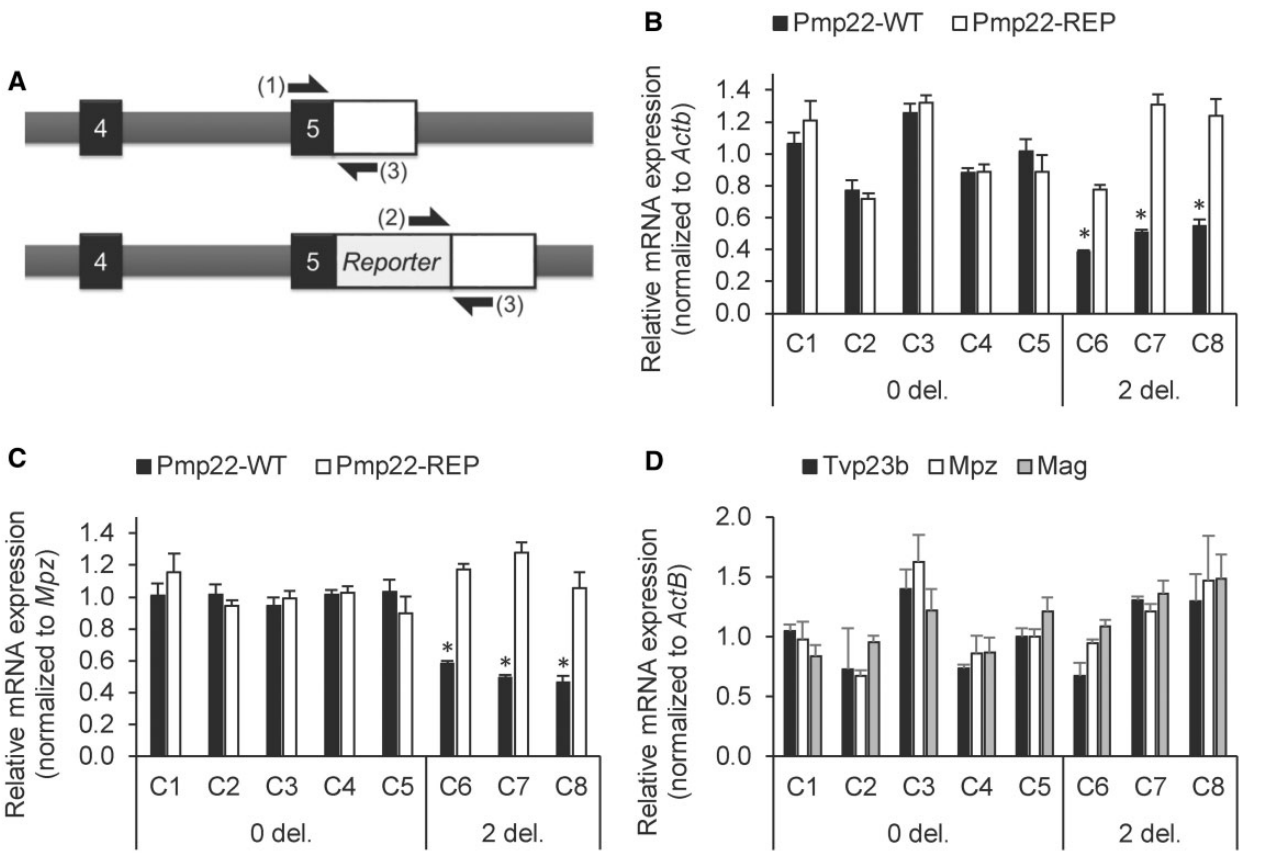

Figure 3. Pmp22-SE drives approximately half of total *Pmp22* transcription in S16 cells. (**A**) Uniquely-positioned forward primers [position 1 and 2, Pmp22 wild-type allele (Pmp22-WT) Forward or Pmp22 reporter allele (Pmp22-REP) Forward] and similarly-positioned reverse primers (position 3, Pmp22-WT Reverse and Pmp22-REP Reverse) were used to measure unique PCR products from two distinct types of *Pmp22* alleles, referred to as the wild-type alleles (lacking the reporter) or the reporter allele. (**B** and **C**) Expression analysis indicates the expression levels of the Pmp22 alleles in clones C6–C8 normalized to either *Actb* (B) or myelin protein zero (*Mpz*, C) relative to clones C1–C5 which do not possess any deletion of Pmp22-SE. (**D**) Relative expression levels are shown for *Tvp23b*, the next closest expressed gene to Pmp22-SE, and myelin genes *Mpz* and myelin-associated glycoprotein (*Mag*). In all cases, expression levels are shown relative to the average of clones C1–C5, which was set as 1. Error bars represent the standard deviation of three independent measurements for clones C1 and C3–C8 and two measurements for clone C2. Statistical analysis denotes results for biological replicates comparing the mean of the zero-deletion clones ($n = 5$) to the mean of the two-deletion clones ($n = 3$) (*$P < 0.05$).

varies by as much as 30% when normalized to *Actb* expression, we also normalized expression of *Pmp22* to expression of the highly expressed myelin protein zero (*Mpz*) gene (Fig. 3C), which is regulated by many of the same transcription factors as *Pmp22* (35,43) and would therefore be expected to show similar changes in expression if the reduced expression in clones C6–C8 is due to upstream differences in pro-myelinating transcription factors. A similar allele-specific reduction of Pmp22 was observed using *Mpz* normalization with an apparent reduction in clone-to-clone variability, while the normalized reporter allele expression was unchanged from parental and control lines.

While our analysis employed three independent clones in which 2 of the 3 *Pmp22* alleles had deletion of the super-enhancer, we had also obtained clones C11 and C12 in which 1 of the 3 alleles have a similar deletion of Pmp22-SE (Supplementary Material, Fig. S3). C11 displayed an approximate 25% reduction of *Pmp22* levels specific to the wild-type alleles, while expression from the reporter allele was unchanged compared to the parental cell line and clone C10, in which no deletion could be detected. These data suggest that one of C11's two wild-type alleles possesses a deletion of Pmp22-SE. By contrast, clone C12 displayed a 50% reduction of *Pmp22* levels unique to the reporter allele with unaffected wild-type allele expression, indicating that the deletion of Pmp22-SE occurred on the reporter allele in this clone. Together, these data are consistent with the conclusion that each copy of Pmp22-SE is responsible for approximately half of *Pmp22* transcription from the copy of chromosome 10 on which it is located.

To evaluate whether these effects were specific to *Pmp22*, we measured expression of other myelin genes *Mpz* and myelin-associated glycoprotein (*Mag*), which are regulated by similar transcription factors like SOX10 and EGR2 (28). The reduction of expression appears unique to *Pmp22*, as other myelin genes displayed no consistent trend in expression relative to the negative clones (Fig. 3D). As an additional measure of specificity, we analyzed expression of the gene *Tvp23b*, which is located approximately 100 kb upstream of Pmp22-SE and is therefore the second most proximal expressed gene to the super-enhancer, in order to determine whether Pmp22-SE's apparent regulation of *Pmp22* was potentially due to proximity. As with *Mpz* and *Mag*, deletion of Pmp22-SE had no apparent effect on *Tvp23b* expression, demonstrating that this region specifically regulates *Pmp22*.

Regulation of the Schwann cell-specific P1 promoter by Pmp22-SE

Pmp22 is primarily transcribed using one of two alternative promoters (47). The P1 promoter driving exon 1A expression is largely Schwann cell-specific and accounts for half of Schwann cell *Pmp22* transcripts in humans and ~75% of transcripts in rodents. The P2 promoter driving exon 1B-containing transcripts is the primary promoter used in other tissues in which *Pmp22* is transcribed, and also drives the majority of *Pmp22* transcription in cultured Schwann cell lines including S16 cells (42). Both promoters are developmentally regulated in peripheral nerve (47), and Pmp22-SE's constituent enhancers are marked by H3K27ac as early as postnatal day one (29); however, Pmp22-SE is particularly correlated with the P1 promoter, as other cell types such as oligodendrocytes that transcribe *Pmp22* only through the P2 promoter also lack this enhancer cluster (29).

Therefore, we tested whether deletion of Pmp22-SE displayed differential effects on transcripts from each promoter. As P2-driven expression accounts for the vast majority of transcripts in our cell lines, the expression level of this transcript mirrors the trend in overall *Pmp22* expression; in clones possessing two deletions of Pmp22-SE, we found that P2 transcripts are down approximately two-fold when normalized to both *Actb* (Fig. 4A) and *Mpz* (Fig. 4B). However, we found that loss of two copies of Pmp22-SE dramatically reduced expression of the Schwann cell-specific P1 promoter.

Because these promoter-specific data would reflect all three copies of *Pmp22*, we sought to independently measure promoter-specific transcription in an allele type-specific manner. We performed qRT-PCR with primer sets spanning the ORF of Pmp22 so that we could differentiate P1 and P2 transcripts in both wild-type and reporter alleles (Fig. 4C). Since the PCR products would be approximately 450 bp in length, we utilized relative standard curve analysis to correct for the reduced amplification efficiency of these PCR products. We found that these results were consistent with our earlier observations; P1-driven transcription on the wild-type alleles was greatly reduced, while P1-driven transcripts from the reporter allele were slightly reduced, though still comparable to the range of P1 transcription observed in our negative clones (Fig. 4D). Similarly, our measurements show that the observed reduction of P2-driven transcription is only present on the wild-type alleles (Fig. 4E).

Regulation of the *Pmp22* gene by YY1

Recent studies of enhancer-promoter looping have identified the YY1 transcription factor as critical factor in mediating the function of such loops (48). The YY1 transcription factor was previously shown to regulate *Pmp22* expression with Schwann cell-specific deletion of the YY1 gene (49), and we reasoned that YY1 may promote formation of the predicted loop between the *Pmp22* gene and the distal Pmp22-SE. Accordingly, YY1 binding in the *PMP22* promoter and super-enhancer regions has been detected by ChIP in the ENCODE profiles of transcription factor binding (50,51). Therefore, we used YY1 siRNA to downregulate YY1 levels in the C6 clone and the parental cell line, and as predicted from the *in vivo* studies (49), there was a significant reduction of both wild type and reporter alleles of *Pmp22* in the parental line compared to control siRNA (Fig. 5A). Similarly, transcription from both promoters was dramatically reduced (Fig. 5B). As the reporter and wild type alleles were both sensitive to loss of YY1 in this clone, these data suggest that the role of YY1 in *Pmp22* regulation is not strictly limited to bridging the distal super-enhancer and the *Pmp22* gene.

Discussion

The dosage-sensitive nature of the *Pmp22* gene demonstrates the importance in establishing the correct expression level of this gene. This is especially true in light of the identification of duplications that cause mild CMT-like symptoms without including the gene itself (23,24). Here, we report the characterization of a distal *Pmp22* super-enhancer that coincides with these observed duplications and provides an explanation for how these duplications produce CMT-like symptoms.

In this study, we analyzed existing ChIP-seq data sets (26,28,29) and employed the genome editing CRISPR-Cas9 system to identify and delete this super-enhancer *in vitro*. Pmp22-SE drives approximately half of *Pmp22* transcription in this Schwann cell culture model. We presume that the residual amount of Schwann cell *Pmp22* expression is accounted for by

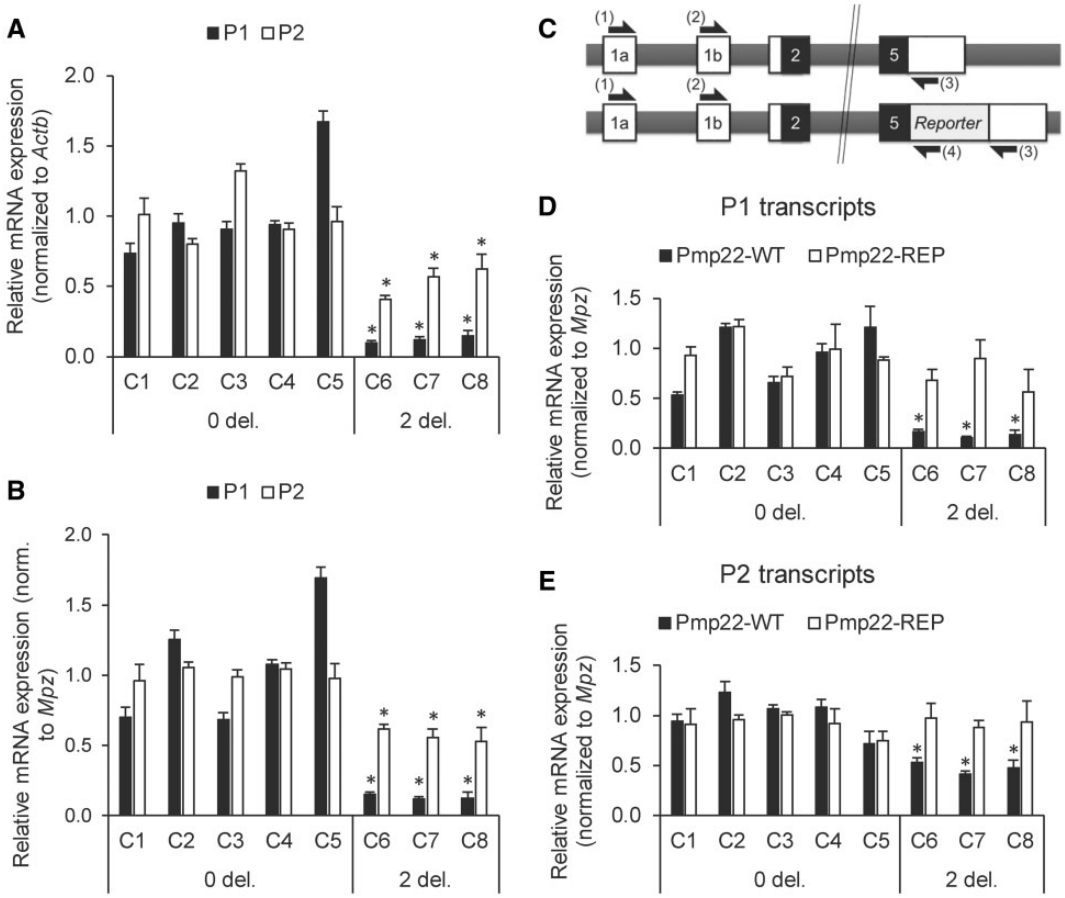

Figure 4. Pmp22-SE is critical for the usage of an alternative Schwann cell-specific promoter. Promoter-specific primer sets were used to determine the relative level of Pmp22 transcripts originating from promoters P1 and P2, incorporating exons 1A and 1B, respectively. Results are presented normalized to expression of both *Actb* (**A**) and *Mpz* (**B**). Levels are shown relative to the average of clones C1–C5 for each promoter, which was set to 1. (**C**) Schematic showing primer placement for whole-transcript amplification using a promoter-specific forward primer (positions 1 and 2, Pmp22-P1 Forward and Pmp22-P2 Forward) and an allele type-specific reverse primer (positions 3 and 4, Pmp22-WT Reverse and Pmp22-REP2 Reverse). (**D** and **E**) Allele type-specific expression for transcripts from the P1 promoter (D) and P2 promoter (E) is shown. Expression for each promoter/allele type combination was calculated using a relative standard curve constructed via serial dilutions of two independent pools of cDNA from the parent line. Error bars represent the standard deviation of three independent measurements for clones C1 and C3–C8 and two measurements for clone C2. Statistical analysis denotes results for biological replicates comparing the mean of the zero-deletion clones ($n = 5$) to the mean of the two-deletion clones ($n = 3$) (*$P < 0.05$).

other enhancers outside of Pmp22-SE. In addition to the late myelination Schwann cell-specific element (LMSE) upstream of the P1 *Pmp22* promoter (22), a highly EGR2-responsive element at +11 kb within *Pmp22*'s largest intron promotes tissue-specific expression of a linked reporter gene (44). In addition, a putative enhancer at -162 kb demonstrates high occupancy of both H3K27ac and TEAD1 binding (29). Therefore, it is likely that Pmp22-SE acts in concert with some combination of these elements to promote full levels of expression.

Interestingly, reduction from the Schwann cell-specific P1 promoter was robustly down-regulated by deletion of Pmp22-SE. ChIP-seq analysis of H3K27ac in oligodendrocytes, which weakly transcribe *Pmp22* exclusively from the P2 promoter, indicated that Pmp22-SE's constituent enhancers are not active in this tissue (29). Additionally, TEAD1, which has been shown to favor expression from the P1 promoter, binds prominently at the 'B' and 'C' sites within Pmp22-SE (29). Taken together with our data, these results suggest that Pmp22-SE plays an important role in selection of the Schwann cell-specific promoter.

A previous study evaluating the importance of YY1 in peripheral nerve myelination showed that this transcription factor functions upstream of EGR2 (49). The broad importance of EGR2 in myelination and *Pmp22* transcriptional regulation may therefore explain why knockdown of YY1 induces down-regulation of *Pmp22* transcription even in the absence of Pmp22-SE. As YY1 binds at the *Pmp22* promoter, it is likely that some combination of these mechanisms governs Pmp22-SE-independent YY1 regulation of *Pmp22*.

While our data suggest a role in cell type-specific promoter usage, our *in vitro* system may not quantitatively recapitulate the role of the super-enhancers at specific developmental stages. However, as ChIP-seq data for H3K27 acetylation indicate that Pmp22-SE's constituent enhancers are established as early as postnatal day one and maintain this mark of activity through the peak period of myelination (29), we can speculate that Pmp22-SE plays an important role in developmental regulation by enabling the occupancy of postnatally regulated pro-myelination transcription factors like EGR2 and TEAD1. Future establishment of a rodent model bearing deletion of Pmp22-SE can shed light on the role of this super-enhancer in developmental upregulation and/or maintenance of *Pmp22* transcription.

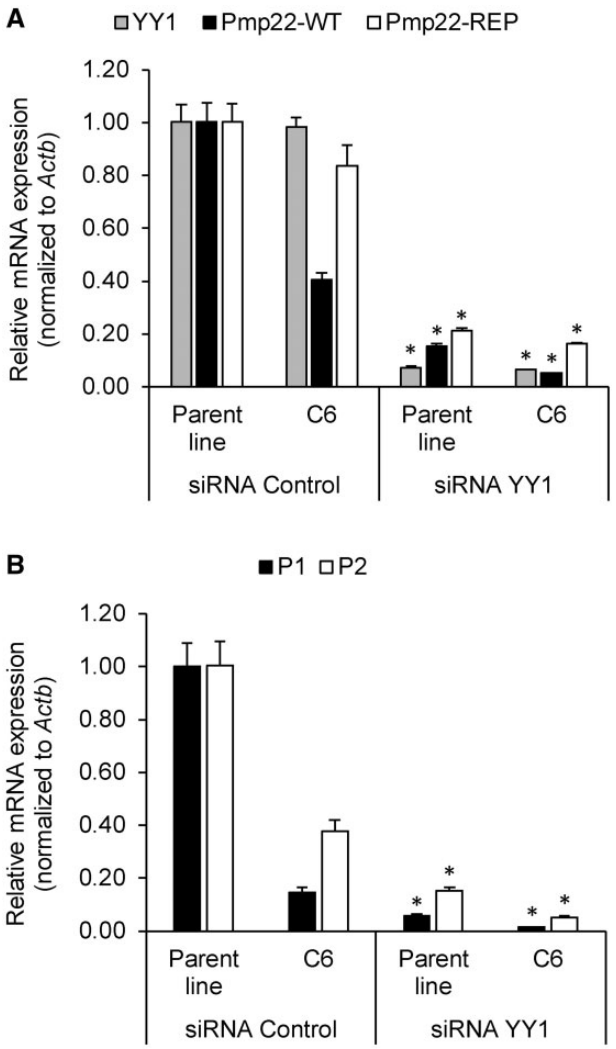

Figure 5. Knockdown of YY1 transcription factor reduces *Pmp22* transcription independent of Pmp22-SE. Allele-specific (**A**) and promoter-specific (**B**) *Pmp22* transcription normalized to *Actb* are shown for cells treated with siRNA targeting the transcription factor *Yy1*. Levels are shown relative to the parent line sample treated with non-targeting control siRNA, each set to 1. Error bars represent the standard deviation of two independent experiments. Statistical analysis denotes significant differences in the YY1 siRNA-treated samples compared to samples treated with control siRNA within the same line (*$P < 0.05$).

In summary, deletion of an enhancer cluster shows a functional link between distal transcription factor binding sites and expression of a critical PNS myelin gene. These findings provide the first evidence that these distal regulatory elements are required for full *Pmp22* transcription. Notably, several sites of high H3K27ac within Pmp22-SE are not associated with detectable binding of transcriptional regulators of *Pmp22* such as EGR2 and SOX10; therefore, there are likely to be additional transcriptional regulators that support the high level of Pmp22 transcription in myelinating Schwann cells.

Materials and Methods

Super-enhancer peak calling and identification

Super-enhancer regions were determined by calling peaks in a Postnatal day 15 (P15) sciatic nerve H3K27ac ChIP-seq data set as described previously (26), then combining enhancers occurring within 12.5 kb of each other into a single larger domain based off the strategy used by Whyte et al. (36). Normalized reads for each region were ranked against the total number of peaks. Cutoff for super-enhancer designation was set at peaks with a tangent slope >1. The supplementary file lists those super-enhancers that exceed a threshold of >1000 normalized reads.

CRISPR construct design

CRISPR guide RNAs were designed using the E-CRISP design tool (52). Oligonucleotides corresponding to identified target sequences were obtained from IDT and subcloned into the pX330 plasmid (53), purchased from Addgene. Sequences for guide RNA were as follows: GACAAGATGGGAATGAATCA and CTGTTCTAC CCTTACTTAGT (upstream site for clones C1–C8); GACCTTG AAGGAGCCCTGACA and CTGGAACTTCCTCGGGACTGT (upstream site, clones C9–C12); GTAAGAGAAGATTCAGGTAGG and CATTCTCTTCTAAGTCCATCC (downstream site).

Cell line culture and generation of CRISPR-Cas9-modified clonal populations

The S16 F2sN cell line was created by using genome editing to insert reporters downstream of the Pmp22 open reading frame as previously described (19) except that the cassette contained three open reading frames corresponding to firefly luciferase, secreted nanoluciferase and Neomycin resistance, each of which is preceded by the 2a ribosome stuttering sequence.

Cells from the S16 rat Schwann cell line-derived reporter line F2SN were cultured in DMEM supplemented with 4.5 g/l glucose, L-glutamine, penicillin, streptomycin and 5% bovine growth serum (Hyclone). F2SN cells were transfected with the pX330 plasmid containing our guide RNA sequence inserts. After 48 h, genomic DNA was collected from transfected populations and screened for detection of a PCR band corresponding to the post-repair junction. Primer sequences for guide RNA target site amplification were as follows: GCCGTCATCCGCATACTAAC and TGCACATTTTGGGATGTGTT (upstream site, clones C1-C8); GCTTTGGACACCAAGCAGTT and TGGCTTGGACACAGCTTAGA (upstream site, clones C9-C12); ACTCCAGAGTGGCGAGTCAT and GGCTTCCCTCTGTAGCTCCT (downstream site)." Populations in which this band could be detected were sorted via flow cytometry at the UW Carbone Cancer Center Flow Cytometry facility to isolate single cells. Genomic DNA from these clones was screened as above to detect clones possessing the intended deletion. Sanger sequencing was performed with the assistance of the UW-Madison Biotechnology Center to validate the expected repair junction.

Measurement of relative Pmp22-SE copy number

Relative copy number was evaluated using qPCR. Genomic DNA was harvested from confluent cells and assayed using a primer set within Pmp22-SE (TGGCTACAGCAGCTCTCCTT and AGTGGCTCGGTCCTTGACTA) and a primer set in the nearby extragenic space between Pmp22-SE and the Tekt3 gene (AGGGCCTCTTTCCTGAGAAC and TGGCTCTAAGGTCAGGG TGT). The comparative Ct method was used to calculate relative copy number (54).

siRNA treatment

Cells were transfected with siRNA targeting *Yy1* (Ambion, s128676) or a negative siRNA control (IDT, DS NC1) using the

Table 1. Primers used for qRT-PCR

Gene	Forward	Reverse
Actb	CCTAGCACCATGAAGATCAAGA	CTCATCGTACTCCTGCTTGC
Tvp23b	CAGGGTGGGATGTTGTGTTT	CACGTTGCTGTCACAGGACT
Mpz	CCCTGGCCATTGTGGTTTAC	CCATTCACTGGACCAGAAGGAG
Mag	CCTTCCCCAACACCACCTT	TGACGTCCAGACTGGCGTAAC
Yy1	GAGCAGATCATTGGGGAGAA	AGGGAGTTTCTTGCCTGTCA
Pmp22-WT	CGCTGGCCCTCCTTAGT	TACCCTATGCACGCTCAGA
Pmp22-REP	TCGCCTTCTTGACGAGTTCT	ACAGCAATCCCCACTCAACT
Pmp22-REP2	–	TCCACGTCACCGCATGTTAGAAGA
Pmp22-P1	GAGGAAGGGCGTACACCATTG	GGAGTTGGGCTCGGGCT
Pmp22-P2	CGAGTTTGTGCCTGAGGCTAC	AAGCATGGTGGCTGGGAGT

AMAXA 4D-Nucleofector system and SE Cell Line 4D-Nucleofector X Kit L reagents with program DS-138 (Lonza).

RT-qPCR

RNA was harvested from confluent cells or, for siRNA experiments, at 48h after transfection in triplicate using Tri Reagent (Ambion). RNA was converted to cDNA using the M-MLV reverse transcriptase (Invitrogen). cDNAs were analyzed by RT-qPCR using Power SYBR Green Master Mix (Thermo Fisher Scientific) on the StepOnePlus system or the ViiA7 system (Applied Biosystems). Relative expression was calculated using a relative standard curve or the Comparative Ct method (54). Primers used are included in Table 1. Note that for the *Pmp22* reading frame experiment (Fig. 5), an individual reverse primer targeting the 2a sequence was used.

Spectral karyotyping

Metaphase slide preparations were made from the S16 (ATCC® CRL-2941™) cell line, after mitotic arrest with Colcemid (0.015 μg/ml, 2 h) (GIBCO, Gaithersburg, MD), hypotonic treatment (0.075 mol/l KCl, 20 min, 37°C) and fixation with methanol–acetic acid (3: 1). We used commercial SKY probe (Applied Spectral Imaging INC, Carlsbad, CA) allowing the visualization of the individually colored chromosomes (55,56). This technique is used to identify structural and numerical chromosome aberrations in this rat cell line.

Statistical analysis

P-values were obtained from the Student's two-tailed *t*-test ($P < 0.05$ is considered to be statistically significant).

Supplementary Material

Supplementary Material is available at *HMG* online.

Acknowledgements

We wish to thank members of our lab for feedback on this study.

Conflict of Interest statement. None declared.

Funding

This work was supported by the National Institutes of Health [RO1 NS083841 to J.S. and U54 core grant HD090256; T32 GM008688 to H.P.].

References

1. Nave, K.A. and Salzer, J.L. (2006) Axonal regulation of myelination by neuregulin 1. *Curr. Opin. Neurobiol.*, **16**, 492–500.
2. Taveggia, C., Zanazzi, G., Petrylak, A., Yano, H., Rosenbluth, J., Einheber, S., Xu, X., Esper, R.M., Loeb, J.A., Shrager, P. *et al.* (2005) Neuregulin-1 type III determines the ensheathment fate of axons. *Neuron*, **47**, 681–694.
3. Hopkins, J.M. and Bunge, R.P. (1991) Regeneration of axons from adult human retina in vitro. *Exp. Neurol.*, **112**, 243–251.
4. Suter, U. and Scherer, S.S. (2003) Disease mechanisms in inherited neuropathies. *Nat. Rev. Neurosci.*, **4**, 714–726.
5. Skre, H. (1974) Genetic and clinical aspects of Charcot-Marie-Tooth's disease. *Clin. Genet.*, **6**, 98–118.
6. Lupski, J.R., de Oca-Luna, R.M., Slaugenhaupt, S., Pentao, L., Guzzetta, V., Trask, B.J., Saucedo-Cardenas, O., Barker, D.F., Killian, J.M., Garcia, C.A. *et al.* (1991) DNA duplication associated with Charcot-Marie-Tooth disease type 1A. *Cell*, **66**, 219–232.
7. Raeymaekers, P., Timmerman, V., Nelis, E., De Jonghe, P., Hoogenduk, J.E., Baas, F., Barker, D.F., Martin, J.J., De Visser, M., Bolhuis, P.A. and Van Broeckhoven, C. (1991) Duplication in chromosome 17p11.2 in Charcot-Marie-Tooth neuropathy type 1a (CMT 1a). The HMSN Collaborative Research Group. *Neuromuscul. Disord.*, **1**, 93–97.
8. Snipes, G.J., Suter, U., Welcher, A.A. and Shooter, E.M. (1992) Characterization of a novel peripheral nervous system myelin protein (PMP-22/SR13). *J. Cell Biol.*, **117**, 225–238.
9. Patel, P.I., Roa, B.B., Welcher, A.A., Schoener-Scott, R., Trask, B.J., Pentao, L., Snipes, G.J., Garcia, C.A., Francke, U., Shooter, E.M., Lupski, J.R. and Suter, U. (1992) The gene for the peripheral myelin protein PMP-22 is a candidate for Charcot-Marie-Tooth disease type 1A. *Nat. Genet.*, **1**, 159–165.
10. Chance, P.F., Alderson, M.K., Leppig, K.A., Lensch, M.W., Matsunami, N., Smith, B., Swanson, P.D., Odelberg, S.J., Disteche, C.M. and Bird, T.D. (1993) DNA deletion associated with hereditary neuropathy with liability to pressure palsies. *Cell*, **72**, 143–151.
11. Sereda, M., Griffiths, I., Pühlhofer, A., Stewart, H., Rossner, M.J., Zimmermann, F., Magyar, J.P., Schneider, A., Hund, E., Meinck, H.-M., Suter, U. and Nave, K.-A. (1996) A transgenic rat model of Charcot-Marie-Tooth disease. *Neuron*, **16**, 1049–1060.
12. Adlkofer, K., Martini, R., Aguzzi, A., Zielasek, J., Toyka, K.V. and Suter, U. (1995) Hypermyelination and demyelinating peripheral neuropathy in Pmp22-deficient mice. *Nat. Genet.*, **11**, 274–280.
13. Adlkofer, K., Frei, R., Neuberg, D.H., Zielasek, J., Toyka, K.V. and Suter, U. (1997) Heterozygous peripheral myelin protein

22-deficient mice are affected by a progressive demyelinating tomaculous neuropathy. *J. Neurosci.*, **17**, 4662–4671.
14. Guo, J., Wang, L., Zhang, Y., Wu, J., Arpag, S., Hu, B., Imhof, B.A., Tian, X., Carter, B.D., Suter, U. and Li, J. (2014) Abnormal junctions and permeability of myelin in PMP22-deficient nerves. *Ann. Neurol.*, **75**, 255–265.
15. Sereda, M.W., Meyer zu Horste, G., Suter, U., Uzma, N. and Nave, K.A. (2003) Therapeutic administration of progesterone antagonist in a model of Charcot-Marie-Tooth disease (CMT-1A). *Nat. Med.*, **9**, 1533–1537.
16. Passage, E., Norreel, J., Noack-Fraissignes, P., Sanguedolce, V., Pizant, J., Thirion, X., Robaglia-Schlupp, A., Pellissier, J. and Fontés, M. (2004) Ascorbic acid treatment corrects the phenotype of a mouse model of Charcot-Marie-Tooth disease. *Nat. Med.*, **10**, 396–401.
17. Perea, J., Robertson, A., Tolmachova, T., Muddle, J., King, R., Ponsford, S., Thomas, P. and Huxley, C. (2001) Induced myelination and demyelination in a conditional mouse model of Charcot-Marie-Tooth disease type 1A. *Hum. Mol. Genet.*, **10**, 1007–1018.
18. Zhao, H.T., Damle, S., Ikeda-Lee, K., Kuntz, S., Li, J., Mohan, A., Kim, A., Hung, G., Scheideler, M.A., Scherer, S.S. *et al.* (2017) PMP22 antisense oligonucleotides reverse Charcot-Marie-Tooth disease type 1A features in rodent models. *J. Clin. Invest.*, **128**, 359–368.
19. Inglese, J., Dranchak, P., Moran, J.J., Jang, S.-W., Srinivasan, R., Santiago, Y., Zhang, L., Guha, R., Martinez, N., MacArthur, R. *et al.* (2014) Genome editing-enabled HIS assays expand drug target pathways for Charcot-Marie-Tooth disease. *ACS Chem. Biol.*, **9**, 2594–2602.
20. Jang, S.W., Lopez-Anido, C., MacArthur, R., Svaren, J. and Inglese, J. (2012) Identification of drug modulators targeting gene-dosage disease CMT1A. *ACS. Chem. Biol.*, **7**, 1205–1213.
21. Maier, M., Berger, P., Nave, K.A. and Suter, U. (2002) Identification of the regulatory region of the peripheral myelin protein 22 (PMP22) gene that directs temporal and spatial expression in development and regeneration of peripheral nerves. *Mol. Cell. Neurosci.*, **20**, 93–109.
22. Maier, M., Castagner, F., Berger, P. and Suter, U. (2003) Distinct elements of the peripheral myelin protein 22 (PMP22) promoter regulate expression in Schwann cells and sensory neurons. *Mol. Cell. Neurosci.*, **24**, 803–817.
23. Weterman, M.A., van Ruissen, F., de Wissel, M., Bordewijk, L., Samijn, J.P., van der Pol, W.L., Meggouh, F. and Baas, F. (2010) Copy number variation upstream of PMP22 in Charcot-Marie-Tooth disease. *Eur. J. Hum. Genet.*, **18**, 421–428.
24. Zhang, F., Seeman, P., Liu, P., Weterman, M.A., Gonzaga-Jauregui, C., Towne, C.F., Batish, S.D., De Vriendt, E., De Jonghe, P., Rautenstrauss, B. *et al.* (2010) Mechanisms for nonrecurrent genomic rearrangements associated with CMT1A or HNPP: rare CNVs as a cause for missing heritability. *Am. J. Hum. Genet.*, **86**, 892–903.
25. Lopez-Anido, C., Sun, G., Koenning, M., Srinivasan, R., Hung, H.A., Emery, B., Keles, S. and Svaren, J. (2015) Differential Sox10 genomic occupancy in myelinating glia. *Glia*, **63**, 1897–1914.
26. Hung, H.A., Sun, G., Keles, S. and Svaren, J. (2015) Dynamic regulation of Schwann cell enhancers after peripheral nerve injury. *J. Biol. Chem.*, **290**, 6937–6950.
27. Creyghton, M.P., Cheng, A.W., Welstead, G.G., Kooistra, T., Carey, B.W., Steine, E.J., Hanna, J., Lodato, M.A., Frampton, G.M., Sharp, P.A. *et al.* (2010) Histone H3K27ac separates active from poised enhancers and predicts developmental state. *Proc. Natl. Acad. Sci. U. S. A.*, **107**, 21931–21936.
28. Srinivasan, R., Sun, G., Keles, S., Jones, E.A., Jang, S.W., Krueger, C., Moran, J.J. and Svaren, J. (2012) Genome-wide analysis of EGR2/SOX10 binding in myelinating peripheral nerve. *Nucleic Acids Res.*, **40**, 6449–6460.
29. Lopez-Anido, C., Poitelon, Y., Gopinath, C., Moran, J.J., Ma, K.H., Law, W.D., Antonellis, A., Feltri, M.L. and Svaren, J. (2016) Tead1 regulates the expression of Peripheral Myelin Protein 22 during Schwann cell development. *Hum. Mol. Genet.*, **25**, 3055–3069.
30. Britsch, S., Goerich, D.E., Riethmacher, D., Peirano, R.I., Rossner, M., Nave, K.A., Birchmeier, C. and Wegner, M. (2001) The transcription factor Sox10 is a key regulator of peripheral glial development. *Genes Dev.*, **15**, 66–78.
31. Finzsch, M., Schreiner, S., Kichko, T., Reeh, P., Tamm, E., Bösl, M., Meijer, D. and Wegner, M. (2010) Sox10 is required for Schwann cell identity and progression beyond the immature Schwann cell stage. *J. Cell. Biol.*, **189**, 701–712.
32. Topilko, P., Schneider-Maunoury, S., Levi, G., Baron-Van Evercooren, A., Chennoufi, A.B., Seitanidou, T., Babinet, C. and Charnay, P. (1994) Krox-20 controls myelination in the peripheral nervous system. *Nature*, **371**, 796–799.
33. Le, N., Nagarajan, R., Wang, J.Y., Araki, T., Schmidt, R.E. and Milbrandt, J. (2005) Analysis of congenital hypomyelinating Egr2Lo/Lo nerves identifies Sox2 as an inhibitor of Schwann cell differentiation and myelination. *Proc. Natl. Acad. Sci. U. S. A.*, **102**, 2596–2601.
34. Jang, S.W., LeBlanc, S.E., Roopra, A., Wrabetz, L. and Svaren, J. (2006) In vivo detection of Egr2 binding to target genes during peripheral nerve myelination. *J. Neurochem.*, **98**, 1678–1687.
35. Jang, S.W. and Svaren, J. (2009) Induction of myelin protein zero by early growth response 2 through upstream and intragenic elements. *J. Biol. Chem.*, **284**, 20111–20120.
36. Arthur-Farraj, P.J., Latouche, M., Wilton, D.K., Quintes, S., Chabrol, E., Banerjee, A., Woodhoo, A., Jenkins, B., Rahman, M., Turmaine, M. *et al.* (2012) c-Jun reprograms Schwann cells of injured nerves to generate a repair cell essential for regeneration. *Neuron*, **75**, 633–647.
37. Jones, E.A., Brewer, M.H., Srinivasan, R., Krueger, C., Sun, G., Charney, K.N., Keles, S., Antonellis, A. and Svaren, J. (2012) Distal enhancers upstream of the Charcot-Marie-Tooth type 1A disease gene PMP22. *Hum. Mol. Genet.*, **21**, 1581–1591.
38. Whyte, W.A., Orlando, D.A., Hnisz, D., Abraham, B.J., Lin, C.Y., Kagey, M.H., Rahl, P.B., Lee, T.I. and Young, R.A. (2013) Master transcription factors and mediator establish super-enhancers at key cell identity genes. *Cell*, **153**, 307–319.
39. Ma, K.H., Hung, H.A. and Svaren, J. (2016) Epigenomic Regulation of Schwann Cell Reprogramming in Peripheral Nerve Injury. *J. Neurosci.*, **36**, 9135–9147.
40. Heintzman, N.D., Stuart, R.K., Hon, G., Fu, Y., Ching, C.W., Hawkins, R.D., Barrera, L.O., Van Calcar, S., Qu, C., Ching, K.A. *et al.* (2007) Distinct and predictive chromatin signatures of transcriptional promoters and enhancers in the human genome. *Nat. Genet.*, **39**, 311–318.
41. Li, Y., Rivera, C.M., Ishii, H., Jin, F., Selvaraj, S., Lee, A.Y., Dixon, J.R. and Ren, B. (2014) CRISPR reveals a distal super-enhancer required for Sox2 expression in mouse embryonic stem cells. *PLoS One*, **9**, e114485.
42. Hai, M., Muja, N., DeVries, G.H., Quarles, R.H. and Patel, P.I. (2002) Comparative analysis of Schwann cell lines as model systems for myelin gene transcription studies. *J. Neurosci. Res.*, **69**, 497–508.

43. LeBlanc, S.E., Jang, S.W., Ward, R.M., Wrabetz, L. and Svaren, J. (2006) Direct regulation of myelin protein zero expression by the Egr2 transactivator. *J. Biol. Chem.*, **281**, 5453–5460.
44. Jones, E.A., Lopez-Anido, C., Srinivasan, R., Krueger, C., Chang, L.W., Nagarajan, R. and Svaren, J. (2011) Regulation of the PMP22 Gene through an Intronic Enhancer. *J. Neurosci.*, **31**, 4242–4250.
45. Goda, S., Hammer, J., Kobiler, D. and Quarles, R.H. (1991) Expression of the myelin-associated glycoprotein in cultures of immortalized Schwann cells. *J. Neurochem.*, **56**, 1354–1361.
46. Fang, J., Qian, J.J., Yi, S., Harding, T.C., Tu, G.H., VanRoey, M. and Jooss, K. (2005) Stable antibody expression at therapeutic levels using the 2A peptide. *Nat. Biotechnol.*, **23**, 584–590.
47. Suter, U., Snipes, G.J., Schoener-Scott, R., Welcher, A.A., Pareek, S., Lupski, J.R., Murphy, R.A., Shooter, E.M. and Patel, P.I. (1994) Regulation of tissue-specific expression of alternative peripheral myelin protein-22 (PMP22) gene transcripts by two promoters. *J. Biol. Chem.*, **269**, 25795–25808.
48. Weintraub, A.S., Li, C.H., Zamudio, A.V., Sigova, A.A., Hannett, N.M., Day, D.S., Abraham, B.J., Cohen, M.A., Nabet, B., Buckley, D.L. *et al.* (2017) YY1 is a structural regulator of enhancer-promoter loops. *Cell*, **171**, 1573–1588.
49. He, Y., Kim, J.Y., Dupree, J., Tewari, A., Melendez-Vasquez, C., Svaren, J. and Casaccia, P. (2010) Yy1 as a molecular link between neuregulin and transcriptional modulation of peripheral myelination. *Nat. Neurosci.*, **13**, 1472–1480.
50. Cheng, C., Alexander, R., Min, R., Leng, J., Yip, K.Y., Rozowsky, J., Yan, K.K., Dong, X., Djebali, S., Ruan, Y. *et al.* (2012) Understanding transcriptional regulation by integrative analysis of transcription factor binding data. *Genome Res.*, **22**, 1658–1667.
51. Gerstein, M.B., Kundaje, A., Hariharan, M., Landt, S.G., Yan, K.K., Cheng, C., Mu, X.J., Khurana, E., Rozowsky, J., Alexander, R. *et al.* (2012) Architecture of the human regulatory network derived from ENCODE data. *Nature*, **489**, 91–100.
52. Heigwer, F., Kerr, G. and Boutros, M. (2014) E-CRISP: fast CRISPR target site identification. *Nat. Methods*, **11**, 122–123.
53. Cong, L., Ran, F.A., Cox, D., Lin, S., Barretto, R., Habib, N., Hsu, P.D., Wu, X., Jiang, W., Marraffini, L.A. *et al.* (2013) Multiplex genome engineering using CRISPR/Cas systems. *Science*, **339**, 819–823.
54. Livak, K.J. and Schmittgen, T.D. (2001) Analysis of relative gene expression data using real-time quantitative PCR and the 2(-Delta Delta C(T)) Method. *Methods*, **25**, 402–408.
55. Schröck, E., du Manoir, S., Veldman, T., Schoell, B., Wienberg, J., Ferguson-Smith, M.A., Ning, Y., Ledbetter, D.H., Bar-Am, I., Soenksen, D. *et al.* (1996) Multicolor spectral karyotyping of human chromosomes. *Science*, **273**, 494–497.
56. Buwe, A., Steinlein, C., Koehler, M.R., Bar-Am, I., Katzin, N. and Schmid, M. (2003) Multicolor spectral karyotyping of rat chromosomes. *Cytogenet. Genome. Res.*, **103**, 163–168.